Dynamics of multiple-junction stacked flux-flow oscillators: Comparison between theory and experiment

Shigeki Sakai
Electrotechnical Laboratory, 1-1-4 Umezono, Tsukuba-shi, Ibaraki 305, Japan

Alexey V. Ustinov
Physikalisches Institut III, Universität Erlangen-Nürnberg, D-91058 Erlangen, Germany

Norbert Thyssen and Hermann Kohlstedt
Institute of Thin Film and Ion Technology, Forschungszentrum Jülich, D-52425 Jülich, Germany
(Received 11 February 1998)

Flux-flow dynamics in long N-layered Nb/Al-AlO_x/Nb Josephson tunnel junctions is investigated experimentally and by numerical simulations. Magnetic-field-dependent current-voltage characteristics show the collective flow of Josephson vortices in the experiments with $N=7$ and $N=9$. In order to interpret the observed characteristics we performed numerical analysis using a finite difference method. The structure of cavitylike resonances displayed in the I-V characteristics is accounted for by the characteristic frequencies calculated using the coupled sine-Gordon equations model. A static I-V curve obtained numerically for a seven-junction stack shows voltage-locked flux-flow motion among the inner five junctions. The numbers of vortices in the top and bottom junction is found to be larger than those of the inner junctions because of the thicker top and bottom Nb electrodes. Numerical data show very good overall agreement with the experiment. [S0163-1829(98)02533-8]

I. INTRODUCTION

Long Josephson junctions operated in the flux-flow mode are presently being successfully used as local oscillators in integrated submillimeter-wave receivers.[1] Mutually phase-locked oscillators increase the output power and decrease the linewidth, which improves the performance of such devices. Vertical stacking of Josephson junctions appears as natural realization of such oscillators. The coupling effects between junctions appear if the superconducting layer thickness in a stack is equal or smaller than the London penetration depth. In comparison with planar oscillator arrays, the mutual inductive coupling in stacks can be by several orders of magnitude stronger. In addition, the impedance of a stack is higher than that of a single-layer junction. Studies of twofold stacks[2] have already shown promising phase-locking behavior with possible in-phase and out-of-phase oscillations in the two junctions.

The theoretical model developed for stacked Josephson junctions[3] is proved to be a very useful tool for understanding the dynamics of stacks. In this model the stacked system is represented by a set of coupled sine-Gordon equations with quasiparticle tunneling loss and bias current terms. The coupling occurs ''nductively'' in the following sense. The supercurrent in a superconducting layer (S layer) is induced by a magnetic field in an insulating layer adjacent to one side of the S layer so that it shields the magnetic-field penetration inside the S layer. If the thickness of the S layer is equal or less than the London penetration depth, this shielding current does not decay to the opposite side of the S layer, to which another insulating layer is connected. The spatial derivative of the phase difference in a Josephson junction of a stack is governed by the magnetic field in its insulating barrier and the supercurrents flowing in its electrodes formed by two S layers. Therefore, the spatial derivative of the Josephson phase difference depends not only on the magnetic field in its insulating layer but also on the fields in the adjacent two insulating layers.

Using the model,[3] detailed quantitative comparison of its predictions with experimental data for two- and three-fold stacks was made and good agreement was found.[4,5] Recently, experimental results of flux flow in $Ba_2Sr_2CaCu_2O_{8+y}$ (BSCCO) has also been successfully explained.[6] Detailed experiments with multilayer stacks[7,8] showed rather complex

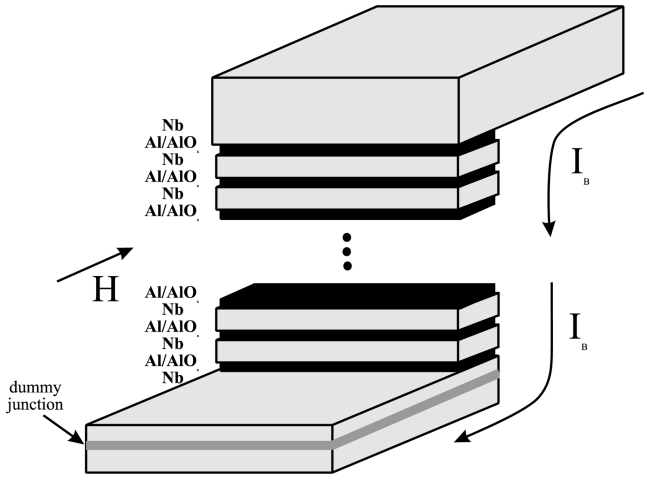

FIG. 1. Stack of long Josephson junctions of the overlap geometry. In a typical experiment the magnetic field H is applied in the plane of the tunnel barriers and the bias current I_B flows across them. The ''dummy junction'' layer is the essential part of the technological procedure described in Sec. III.

dynamics which needs to be interpreted using detailed numerical modeling of these systems.

II. MODEL AND NUMERICAL PROCEDURE

A Josephson-junction stack consisting of N junctions ($i=1,\ldots,N$) contains $N+1$ superconducting layers (numbered $i=0,\ldots,N$). Such a multiple-junction stack of the overlap geometry is sketched in Fig. 1. It consists of alternating superconducting and isolating layers. In a magnetic field H applied parallel to the layers, fluxons penetrate into different Josephson junctions and, under the influence of the bias current I_B may move coherently due to the interaction of their screening currents flowing in the inner superconducting layers. The system of equations which describes the Josephson phase dynamics in the stack can be written in the following form:[3]

$$\frac{\Phi_0}{2\pi\mu_0}\frac{\partial^2}{\partial x^2}\begin{pmatrix}\phi_1\\ \vdots\\ \phi_i\\ \vdots\\ \phi_N\end{pmatrix}=\begin{bmatrix} d_1' & s_1 & 0 & 0 & 0 & 0 & 0\\ s_1 & d_2' & s_2 & 0 & 0 & 0 & 0\\ 0 & \ddots & \ddots & \ddots & 0 & 0 & 0\\ 0 & 0 & s_{i-1} & d_i' & s_i & 0 & 0\\ 0 & 0 & 0 & \ddots & \ddots & \ddots & 0\\ 0 & 0 & 0 & 0 & s_{N-2} & d_{N-1}' & s_{N-1}\\ 0 & 0 & 0 & 0 & 0 & s_{N-1} & d_N' \end{bmatrix}\begin{pmatrix}J_1^Z\\ \vdots\\ J_i^Z\\ \vdots\\ J_N^Z\end{pmatrix}, \tag{1}$$

where ϕ_i is the superconducting phase difference on the junction number j and Φ_0 is the magnetic flux quantum. The coupling is determined by the parameters:

$$d_i'=d_i+\lambda_{i-1}\coth\frac{t_{i-1}}{\lambda_{i-1}}+\lambda_i\coth\frac{t_i}{\lambda_i} \quad \text{and} \quad s_i=\frac{-\lambda_i}{\sinh(t_i/\lambda_i)}, \tag{2}$$

where d_i is the tunnel barrier thickness between superconducting layers i and $i-1$, t_i and λ_i are the thickness of the superconducting layer number i and its London penetration depth, respectively. The sum of current components across the junction is

$$J_i^Z=\frac{\Phi_0 C_i}{2\pi}\frac{\partial^2\phi_i}{\partial t^2}+\frac{\Phi_0}{2\pi R_i}\frac{\partial\phi_i}{\partial t}+j_{c,i}\sin(\phi_i)-I_B. \tag{3}$$

Here C_i, R_i, $j_{c,i}$, and I_B are the junction capacitance, resistance, critical current, and bias current densities, respectively. We will consider the case of individual junction voltages being much smaller than the gap voltage corresponding to the superconducting energy gap, thus we assume R_i to be constants. Also, for simplicity in Eq. (3) we ignore the loss term (β term) which accounts for dissipative high-frequency currents in superconducting electrodes.

Numerical simulations were made by solving the system of equations (1) by a finite-difference method. The boundary conditions for the applied magnetic field are given by

$$\begin{aligned}-\left.\frac{\partial\phi_i}{\partial x}\right|_{x=0,L}&=\frac{2\pi\mu_0 H}{\Phi_0}(s_{i-1}+d_i'+s_i)\\ &=\frac{2\pi\mu_0 H}{\Phi_0}\left[d_i+\lambda_{i-1}\tanh\left(\frac{t_{i-1}}{2\lambda_{i-1}}\right)\right.\\ &\quad\left.+\lambda_i\tanh\left(\frac{t_i}{2\lambda_i}\right)\right],\end{aligned} \tag{4}$$

for $i=1,2,\ldots,N$. In order to avoid confusion of using normalized units for a variety of wave propagation cases of a stacked system, we adopted true physical units in the simulation scheme.

Introducing F as the inverse matrix of the matrix in Eq. (1), we obtain

$$\frac{\Phi_0 C_i}{2\pi}\frac{\partial^2\phi_i}{\partial t^2}+\frac{\Phi_0}{2\pi R_i}\frac{\partial\phi_i}{\partial t}=I_B-j_{c,i}\sin(\phi_i)+\frac{\Phi_0}{2\pi\mu_0}\sum_{j=1}^{N}F_{i,j}\frac{\partial^2\phi_j}{\partial x^2} \tag{5}$$

for $i=1,2,\ldots,N$.

In our program code, the matrix element $F_{i,j}$ is calculated in analytical forms for $N<6$, but for arbitrary N we use a subroutine LSGRR in the numerical library IMSL.[9] The finite-difference procedure in our code is a natural extension to those that have been utilized for solving fluxon dynamics in single-barrier long Josephson junctions. In order to avoid spurious oscillations, the second derivative with respect to x in Eq. (5) was replaced by a finite-difference form using five spatial points instead of three points.[10] Virtual points outside the two edges were introduced in order to satisfy the boundary conditions at every time step. A CRAY computer has been used for long-time simulations of I-V curves. In order to visualize the dynamics of stacked junctions, real time simulations with a personal computer have been performed.

III. EXPERIMENTAL DATA FOR SEVEN-JUNCTION STACKS

Stacked Nb/Al-AlO_x/Nb long Josephson junctions of overlap geometry were prepared using the modified SNAP technology. As we already reported earlier,[7] direct fabrication of the bottom Josephson junction of a stack on a rela-

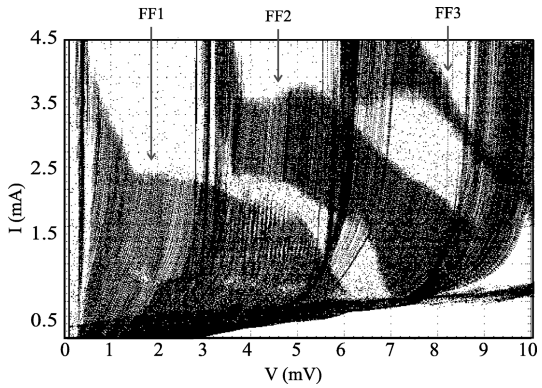

FIG. 2. Flux-flow behavior of the *I-V* characteristics of a seven-fold stack in the varying magnetic field H. Planar dimensions of the stack are $L \times W = 450 \times 10\ \mu m^2$.

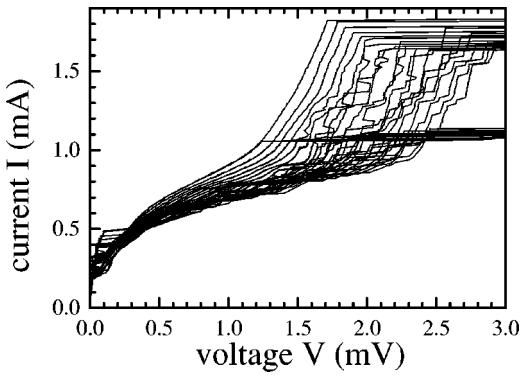

FIG. 3. Measured *I-V* characteristics of seven-fold stack; magnetic field is varied from 8 to 12 Oe with 0.2 Oe increment. Planar dimensions of the stack are $L \times W = 350 \times 20\ \mu m^2$.

tively thick (e.g., 100 nm) bottom Nb electrode always leads to a significantly higher critical current than that of the upper junctions fabricated on thinner Nb layers. This fact appears due to the increase of the surface roughness with film thickness. In order to obtain a small parameter spread between the junctions, we kept constant the oxidation parameters for all junctions and used an Al or Al-AlO_x dummy layer in the base electrode,[11] as shown schematically in Fig. 1. This dummy junction served to compensate the roughness of the thicker base Nb layer. The critical current of the dummy layer is much larger than that of the other tunnel barriers and it does not influence the measurements. Using this process the difference in critical currents is reduced to less than 4%.

The base electrode consisted of a trilayer formed by 102-nm Nb, a thermally oxidized 5-nm Al layer (''dummy junction'') and a 78-nm thick Nb film. Thus, the total thickness of the base electrode of the stack was 185-nm. The stacked Al-AlO_x/Nb junctions were formed on top of the base electrode and consisted of 78 nm Nb layers with Al-AlO_x barriers. The highest Al-AlO_x layer was covered by a 600-nm thick top superconducting electrode. The average critical current density j_c of the junctions was about 380 A/cm^2, which corresponds to the Josephson penetration depth $\lambda_J \approx 20\ \mu m$ calculated for a single-layer junction with thick electrodes. Six different junction sizes were produced on the same wafer. Further details on the fabrication of similar multilayer Nb/Al-AlO_x/Nb junctions and their preliminary measurements have been reported in Refs. 7,8.

Below we mainly focus on the data obtained with $N=7$ stacked junction wafer. Measurements were performed at 4.2 K. *I-V* curves were collected using a digital storage oscilloscope in the external magnetic field H varied from 0 to 40 Oe. An example of *I-V* curves stored during continuous H sweep is shown in Fig. 2. With increasing H, flux-flow branches appear starting from $V=0$ and from various gap voltage branches. In Fig. 2 the individual junction gap branches are seen at the voltages of about $V_1 \approx 2.7$ mV, $V_2 = 2V_1 \approx 5.5$ mV, $V_3 = 3V_1 \approx 8.2$ mV, and so on. At any gap branch some of the junctions in the stack are biased at their gap voltage while the rest of the junctions remains at zero voltage state. With increasing the magnetic field the latter junctions show flux-flow behavior: the flux-flow voltage increases with increasing H. By measuring the flux-flow voltage V_{ff} dependence on H one can roughly evaluate the number of junctions participating in the flux-flow state which turned to be close to the number of layers in the stack. In Fig. 2 one can see that the largest measured flux-flow voltage of the lowest branch marked as ''FF1'' reaches about 6 mV. This is by a factor of about 5 larger than the maximum flux-flow branch voltage of a single-barrier Nb/Al-AlO_x/Nb Josephson junction.

A more detailed region of current-voltage (*I-V*) curves for seven-junction ($L \times W = 350 \times 20\ \mu m^2$) stacks taken in the magnetic-field interval from 8 to 12 Oe is shown in Fig. 3. At low fields the *I-V* curve is rather smooth, resembling a displaced linear slope behavior of a single long Josephson junction.[12] With increasing H, there appear resonant branches with characteristic voltage spacing ΔV of about 110 μV. Similar resonances were observed in stacks of other dimensions and the characteristic voltage spacing between them scaled approximately as L^{-1}. These resonances have too large voltage spacing to be explained by the Fiske resonances of individual junctions. Since stacked junctions are measured in a series, it is not possible to determine individual junction voltages in this experiment. Numerical simulations presented in the following section were performed in order to understand the nature of the resonances and to interpret the collective fluxon dynamics associated with measured *I-V* characteristics.

IV. COMPARISON BETWEEN EXPERIMENT AND NUMERICAL SIMULATIONS

We performed numerical simulations using the model (1) with parameters chosen according to the experiment. The simulation results were obtained without any additional fitting by taking directly the experimental values of the layer thicknesses stated above, junction length $L = 350\ \mu m$, and assuming the London penetration depth $\lambda_L = 100$ nm for all the layers. We used the quasiparticle conductance $G = 6 \times 10^4\ \Omega^{-1}\text{cm}^{-2}$, the capacitance $C = 8.85\ \mu\text{F cm}^{-2}$, and the critical current density $j_c = 380\ \text{A cm}^{-2}$ for all the junctions. Typical time of the bias current ramp during the calculation of one *I-V* curve was about 200 ns in the units of Eq. (5).

Figure 4 shows the simulated *I-V* curves for the magnetic-field interval between 8 and 12 Oe. The presented dc voltage is calculated as the sum of dc voltages of the

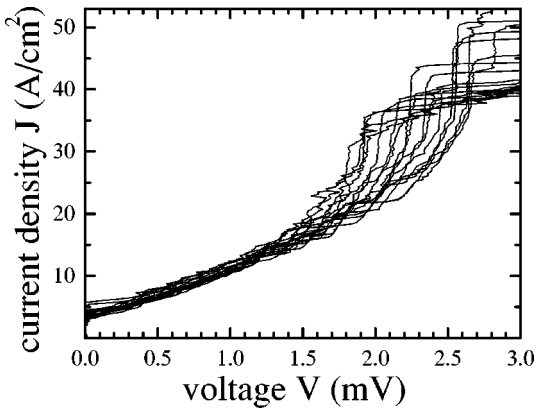

FIG. 4. Numerically simulated *I-V* characteristics; magnetic field changed between 7.6 and 11 Oe with increment 0.2 Oe.

individual junctions in the stack. One can see that, without any additional fitting, the numerically obtained voltage range of the *I-V* characteristics is in remarkably good agreement with the experimental data of Fig. 3. Moreover, the obtained characteristic voltage spacing of about 100 μV between rather well pronounced steps in numerically simulated curves is close to the experimental value $\Delta V \approx 110\ \mu$V.

A numerical procedure allows us to determine the contribution of every junction to the total voltage on the stack. The dc voltages on the individual junctions as functions of the bias current are presented in Fig. 5(a) for a fixed magnetic field of 10.4 Oe. The sum voltage *I-V* curve is shown in Fig. 5(b). One can see that, in addition to the smooth flux-flow dynamics (at low bias current), the individual junction voltages show clear resonant structure of the *I-V* curves. In the bias range of these resonances, approximately between 30 and 50 A cm^{-2}, the top and bottom junctions numbered 1 and 7 have larger voltages than the inner junctions numbered from 2 to 6. The reason for this behavior is due to the much thicker top (600 nm) and bottom (185 nm) electrodes in comparison with the intermediate Nb layers (78 nm).

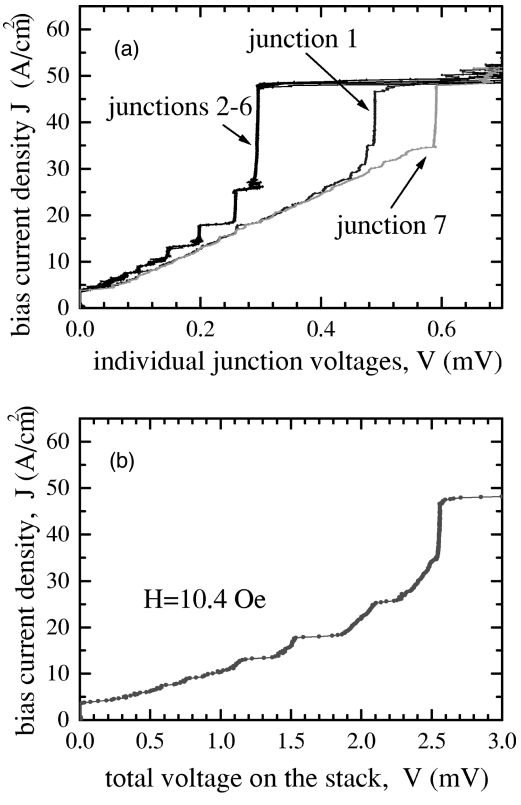

FIG. 5. Simulated *I-V* characteristics for the seven-fold stack: (a) individual junction voltages; (b) total voltage on the stack.

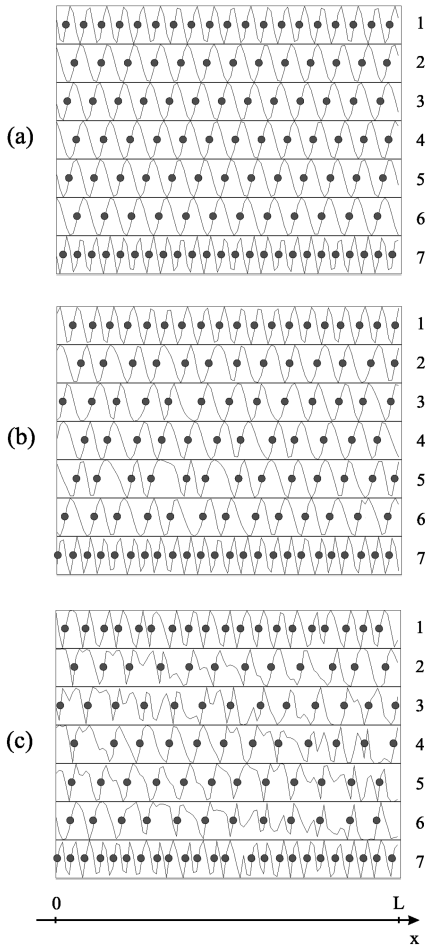

FIG. 6. Snapshots of the simulated flux-flow state in the seven-fold stack. Horizontal scale is the spatial coordinate inside the stack; junctions of different layers are indicated by numbers. Circles correspond to the centers of fluxons defined as the points where the phase difference is equal to $\pi + 2\pi\ m$ with m being an integer. The curves account for the supercurrent distribution $\sin\phi_i(x)$. Bias points correspond to the *I-V* curves shown in Fig. 5: (a) $J = 0\ A/\mathrm{cm}^2$; (b) $J = 13\ A/\mathrm{cm}^2$; (c) $J = 37\ A/\mathrm{cm}^2$.

A detailed analysis of the junction phases simulated at different bias currents for the fixed magnetic field of 10.4 Oe is presented in Fig. 6. This figure shows the snapshots of the supercurrent distribution $\sin\phi_i(x)$: the horizontal scale is the spatial coordinate inside the stack, junctions of different layers are indicated by numbers. Circles correspond to the ''centers of mass'' of fluxons defined as the points where the phase difference ϕ_i is equal to $\pi + 2\pi\ m$ with m being an integer. One can see that at zero-bias current fluxons penetrate all the stacked Josephson layers. The number of fluxons (N_i) in junctions 1, 2–6, and 7 are about 20, 12, and 24, respectively. In the inner junctions 2–6 fluxons form a triangular lattice (checkered pattern). At larger bias currents the

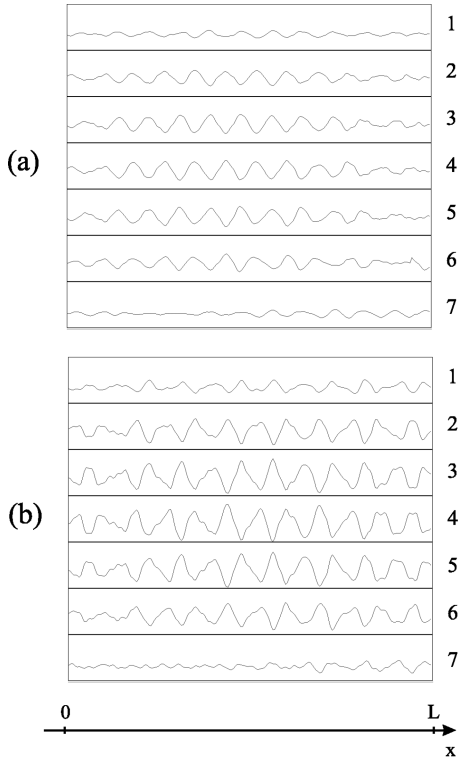

FIG. 7. Simulated dynamic states in the seven-fold stack. Horizontal scale is the spatial coordinate inside the stack; junctions of different layers are indicated by numbers. The curves account for the spatial distribution of the instantaneous voltages $V_i(x) \sim \phi_i(x)$ taken at some arbitrary chosen time. Bias points correspond to the I-V curve at $H = 10.8$ Oe (a) $J = 31\ A/\mathrm{cm}^2$; (b) $J = 44\ A/\mathrm{cm}^2$.

fluxon lattice moves as a whole and its motion generates dc voltage on every junction.

By using these values of N_i, the calculated dc voltages V_i, the junction length L and the equation: $V_i = \Phi_0 (N_i/L) u_i$ for $i = 1-7$, the evaluated fluxon velocities u_i are in the range of $(4.05 \pm 0.06) \times 10^6$ m s^{-1} for all the junctions. This value is very close to the *smallest* characteristic electromagnetic wave velocity of $\overline{c_7} = 4.16 \times 10^6$ m s^{-1} calculated in Refs. 13,4. To illustrate the type of the dynamic mode of the stack, two voltage patterns taken at two bias current levels are shown in Fig. 7. These plots display the spatial distribution of the instantaneous voltages $V_i(x) \propto \phi_i(x)$ taken at some arbitrary chosen time. One can see that among every other junction the positions giving the voltage maxima (or minima) coincide each other, while in the neighboring junctions the oscillations are out of phase with each other. This checkered pattern is the characteristic of the lowest velocity mode $\overline{c_7}$ mentioned above. Thus, the flux-flow dynamics in this regime is accompanied by electromagnetic resonances that are characterized by the lowest characteristic velocity of the seven-fold stack.

However, it is still in question why all junctions are simultaneously locked to some resonant states in spite of the fact that fluxon numbers in junctions 1 and 7 are different from that in junctions 2–6. The number of fluxons in junction 7 is about twice that in junctions 2–6. The fluxon number in junction 1 is close to that of junction 7 but still clearly different.

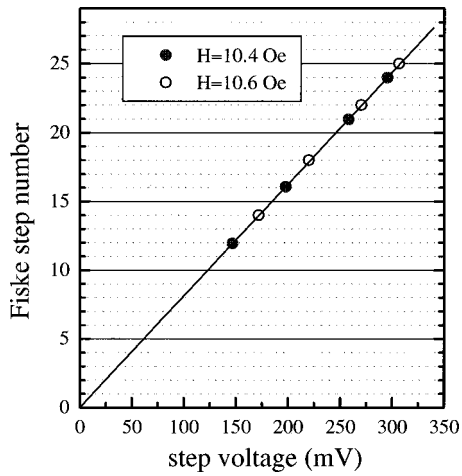

FIG. 8. Fiske step number m versus the voltages of the major voltage-locked resonant steps calculated numerically for the inner junctions of the stack. The straight line corresponds to the Fiske step voltage spacing for the individual junction taken as $\Delta V_{\mathrm{FS}} = 12.3\ \mu$V.

In Fig. 5(a) one can see that, with increasing the bias current from zero, the inner junctions 2–6 of the stack simultaneously lock to several resonant voltage steps at about 147, 198, 258, and 295 μV. These voltages turn out to be very close to be multiple of the expected Fiske step voltage spacing $\Delta V_{\mathrm{FS}} = \Phi_0 \overline{c_7}/(2L) \approx 12.3\ \mu$V of an individual junction of the stack, calculated using the electromagnetic wave propagation velocity $\overline{c_7}$ mentioned above. Figure 8 shows Fiske step numbers m versus the numerically calculated step voltages V_{step} for two values of the magnetic field H. The straight line indicates the theoretically expected slope given by $m = V_{\mathrm{step}}/\Delta V_{\mathrm{FS}}$. From this nearly perfect fit we can conclude that, for this broad velocity range, the flux-flow dynamics in the inner junctions is characterized by cavity resonances (Fiske steps) of the lowest velocity mode $\overline{c_7}$.

The out-of-phase oscillations in the neighboring junctions leads to a very small sum voltage which develops on the whole stack. In Fig. 9, the total voltage at the stack boundary is plotted together with the voltage of one of the junctions.

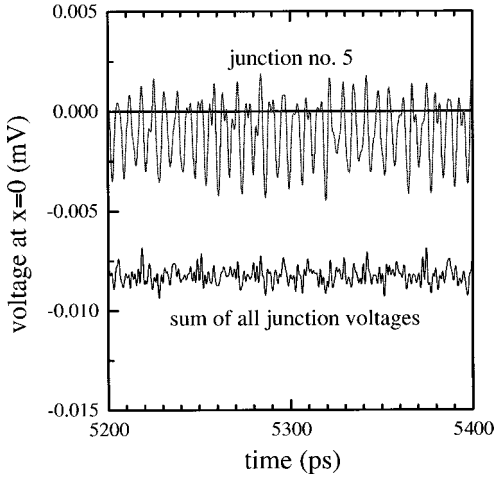

FIG. 9. Simulated time dependence of the voltages at the bias $J = 45\ A/\mathrm{cm}^2$ and magnetic field $H = 10.8$ Oe.

The amplitude of the ac voltage on the whole stack is clearly very small, even smaller than the individual junction voltages.

V. DISCUSSION

Fluxons in coupled long junctions have recently become the subject of intensive theoretical and experimental investigations. The discovery of the intrinsic Josephson effect in some high-temperature superconductors such as BSCCO convincingly showed that these materials are essentially natural superlattices of Josephson junctions formed on the atomic scale.[14–18] The spatial period of such a superlattice is only 1.5 nm, so the Josephson junctions are extremely densely packed. The superconducting electrodes are formed by the copper oxide bilayers as thin as 0.3 nm and are separated by the nonsuperconducting BiO layers.

Superlattices with many Josephson layers can naturally be expected to show very complex dynamics. Therefore, it is important at first to understand in detail the dynamics of stacked junctions with very few layers. In this paper we attempted to apply the theory of inductive coupling in stacks to just few junction layers and found remarkably good agreement with experiment. This suggests that the reliable theoretical model is presently available and realistic simulations of the complex dynamics of stacks with a large number of layers can be done.

Obviously, stacks operated in the out-of-phase oscillation state are of no use for oscillator applications. We note, however, that the stability of other dynamics modes of a stack should depend on actual parameters such as coupling strength, magnetic field, damping, etc., and, in general, one may not exclude the possibility of existing stable oscillation regimes in other modes including the in-phase one. Exploring the parameter space in order to find such regimes is a challenging and important task for the future numerical and experimental investigations.

ACKNOWLEDGMENTS

We would like to thank G. Hechtfischer and R. Kleiner for discussions and also for providing us with their original graphics program code for animated presentation of the phase dynamics. The support of this work by the BMBF Contract No. 13N6945/3 and partial support by Science and Technology Agency (Japan) is gratefully acknowledged. S. S. is grateful to the members of the Institute of Thin Film and Ion Technology at Research Center Jülich and of the Physics Institute III at the University of Erlangen-Nuremberg for their hospitality during his visit. A.V.U. thanks the group members of the Electron Devices Section for the pleasant stay at the Electrotechnical Laboratory (Tsukuba, Japan) and acknowledges the financial support from AIST.

[1] V. P. Koshelets, A. V. Shchukin, S. V. Shitov, and L. V. Filippenko, IEEE Trans. Appl. Supercond. **5**, 3057 (1995).
[2] A. V. Ustinov and H. Kohlstedt, Phys. Rev. B **54**, 6111 (1996).
[3] S. Sakai, P. Bodin, and N. F. Pedersen, J. Appl. Phys. **73**, 2411 (1993).
[4] S. Sakai, A. V. Ustinov, H. Kohlstedt, A. Petraglia, and N. F. Pedersen, Phys. Rev. B **50**, 12 905 (1994).
[5] G. Carapella, G. Costabile, N. F. Pedersen, and S. Sakai (unpublished).
[6] G. Hechtfischer, R. Kleiner, K. Schlenga, W. Walkenhorst, P. Müller, and H. L. Johnson, Phys. Rev. B **55**, 14 638 (1997).
[7] N. Thyssen, A. V. Ustinov, and H. Kohlstedt, J. Low Temp. Phys. **106**, 201 (1997).
[8] N. Thyssen, H. Kohlstedt, and A. V. Ustinov, IEEE Trans. Appl. Supercond. **7**, 2901 (1997).
[9] Numerical subroutine library IMSL: Visual Numerics, Inc., 9990 Richmond Avenue, Suite 400, Houston, TX 77042-4548.
[10] ''*Handbook of Mathematical Functions*, edited by M. Abramowitz and I. A. Stegun (Dover, New York, 1970), p. 884.
[11] H. Kohlstedt, F. König, P. Henne, N. Thyssen, and P. Caputo, J. Appl. Phys. **80**, 5512 (1996).
[12] A. V. Ustinov, H. Kohlstedt, and P. Henne, Phys. Rev. Lett. **77**, 3617 (1996).
[13] R. Kleiner, Phys. Rev. B **50**, 6919 (1994).
[14] R. Kleiner, F. Steinmeyer, G. Kunkel, and P. Müller, Phys. Rev. Lett. **68**, 2394 (1992).
[15] R. Kleiner, P. Müller, H. Kohlstedt, N. F. Pedersen, and S. Sakai, Phys. Rev. B **50**, 3942 (1994).
[16] A. Yurgens, D. Winkler, N. Zavaritsky, and T. Claeson, Phys. Rev. B **53**, R8887 (1996).
[17] Yu. I. Latyshev, J. E. Nevelskaya, and P. Monceau, Phys. Rev. Lett. **77**, 932 (1996).
[18] J. U. Lee, J. E. Nordman, and G. Hohenwarter, Appl. Phys. Lett. **67**, 1471 (1995).